frontiers | Frontiers in Nanotechnology

TYPE Original Research
PUBLISHED 11 August 2025
DOI 10.3389/fnano.2025.1599272

OPEN ACCESS

EDITED BY
Rajeev K. Tyagi,
Institute of Microbial Technology (CSIR), India

REVIEWED BY
Hongwu Sun,
Third Military Medical University, China
Himanshu Paliwal,
Prince of Songkla University, Thailand

*CORRESPONDENCE
Mostafa E. Rateb,
mostafa.rateb@uws.ac.uk

†These authors have contributed equally to this work

RECEIVED 24 March 2025
ACCEPTED 08 July 2025
PUBLISHED 11 August 2025

CITATION
Alhadrami HA, Gamal A, Amaeze N, Sayed AM, Rateb ME and Naguib DM (2025) Enhanced anti-infective activities of sinapic acid through nebulization of lyophilized protransferosomes. *Front. Nanotechnol.* 7:1599272. doi: 10.3389/fnano.2025.1599272

Enhanced anti-infective activities of sinapic acid through nebulization of lyophilized protransferosomes

Hani A. Alhadrami[1,2†], Amr Gamal[3†], Ngozi Amaeze[4], Ahmed M. Sayed[5], Mostafa E. Rateb[6*] and Demiana M. Naguib[7]

[1]Department of Medical Laboratory Sciences, Faculty of Applied Medical Sciences, King Abdulaziz University, Jeddah, Saudi Arabia, [2]King Fahd Medical Research Centre, King Abdulaziz University, Jeddah, Saudi Arabia, [3]Department of Pharmaceutics and Industrial Pharmacy, Faculty of Pharmacy, Beni-Suef University, Beni-Suef, Egypt, [4]School of Health and Life Sciences, University of the West of Scotland, Blantyre, United Kingdom, [5]Department of Pharmacognosy, Faculty of Pharmacy, Nahda University, Beni-Suef, Egypt, [6]School of Computing, Engineering and Physical Sciences, University of the West of Scotland, Paisley, United Kingdom, [7]Department of Pharmaceutics, Faculty of Pharmacy, Nahda University (NUB), Beni-Suef, Egypt

Indroduction: COVID-19 is a contagious illness caused by the virus SARS-CoV-2, a major cause of death globally, even with effective vaccinations. Additionally, multidrug resistant bacterial and fungal pathogens are a real threat to many healthcare settings. Sinapic acid (SA), isolated from different plants or marine algae, has been reported to have antioxidant, antibacterial, and antiviral properties. Although there is evidence that SA has anti-SARS-CoV-2 activity, it is poorly absorbed when taken orally due to its intestinal metabolism. The current study aimed to improve SA's activity against SARS-CoV-2, different bacterial and fungal pathogens, bioavailability, and targeting using a nebulized, freeze-dried, transferosomal formulation.

Methods: A response-surface experimental study using phospholipid, cholesterol, and surfactants was employed to develop transferosomes. Various formulations were prepared and characterized for entrapment efficiency (EE), release, and size to select the optimized formulation. It was then lyophilized into a powder to be evaluated in vivo for its pharmacokinetic properties.

Results and discussion: SA exhibited antibacterial and antifungal activity, with SA-protransferosomes showing enhanced effectiveness compared to that of pure SA and approaching the efficacy of positive controls. Notably, SA protransferosomes demonstrated activity comparable to that of ciprofloxacin against E. faecalis and S. mutans and were effective against Candida albicans and Aspergillus niger, similar to nystatin. The optimized formula significantly enhanced the SARS-CoV-2 activity (IC_{50} = 0.016 ± 0.008 µg/mL), C_{max} by 2.27 times, and AUC (0−∞) by 5.4 times, as compared to pure SA. As a result, the use of nebulized SA-transferosomes can be regarded as a safe and efficient strategy to counter different infections.

KEYWORDS

sinapic acid, SARS-CoV-2, antibacterial, antifungal, transferosomes, nebulizer

1 Introduction

COVID-19, or the novel coronavirus 2019 according to the World Health Organization, is caused by the severe acute respiratory syndrome coronavirus 2 (SARS-CoV-2). Other pandemics caused by different CoVs include severe acute respiratory syndrome (SARS) in 2002–2003 and Middle East Respiratory Syndrome (MERS) in 2012 (Jara et al., 2021). Unfortunately, the COVID-19 pandemic has resulted in more deaths than the previous pandemics combined (Gurwitz, 2020). Worldwide, research organizations have been studying SARS-CoV-2 pandemic since when it was declared. Several successful vaccinations have been reported, and tests on antiviral medications are currently in progress (Adamson et al., 2021).

Antimicrobial resistance (AMR) is a major global health and development threat, responsible for 1.27 million deaths directly and contributing to 4.95 million deaths worldwide in 2019 (Antimicrobial Resistance Collaborators et al., 2022). It affects countries across all regions and income levels, thus posing a significant challenge in the 21st century. The WHO highlighted, among other organisms, the following bacteria on its priority list: *Enterococcus faecalis*, *Streptococcus mutans*, *Escherichia coli*, *Pseudomonas aeruginosa*, *Mycobacterium tuberculosis*, and *Staphylococcus aureus*, all of which pose significant challenges in healthcare settings (WHO, 2024). The rising resistance levels highlight the insufficient development progress and the urgent need for development of new drugs.

Sinapic acid (SA) is a phenolic, acid-containing, natural metabolite found in grapefruits, cranberries, oranges, broccoli, and herbs, such as canola and mustard seed, and seaweed such as *Ulva* sp., *Caulerpa* sp., and *Grateloupia* sp. (Zhong et al., 2020). It is a cinnamic-acid derivative with the chemical structure (3,5-dimethoxy-4-hydroxycinnamic acid) (Pandi and Manickam, 2021). SA was reported to have antioxidant, reno-protective, neuroprotective, anti-inflammatory, hepatoprotective, cardioprotective, antibacterial, anti-cancer, and antiviral properties (Angourani et al., 2023; Hameed et al., 2016). Recently, we reported SA had anti-SARS-CoV-2 activity with an IC_{50} value of 2.69 μg/mL and a minimal cytotoxicity value of 189.3 μg/mL (Orfali et al., 2021). These findings suggested that SA is a good anti-SARS-CoV-2 drug.

Despite SA's comprehensive therapeutic action, its application still needs to be improved because it is slightly soluble in water. In addition, it is metabolized in the intestine, resulting in low oral bioavailability (Pandi and Manickam, 2021; Kern et al., 2003; Shakeel et al., 2016a). To mitigate these limitations, a suitable drug delivery system is required. A few beneficial formulation techniques have been developed in a highly promising, novel sector for SA delivery, including chitosan nanoparticles (Balagangadharan et al., 2019) and a self-nanoemulsifying formulation (Shakeel et al., 2016b).

The pulmonary route provided a wide surface area of approximately 100 m^2 and a non-invasive method of drug administration (Guimarães et al., 2021). Current nanotechnology progress has significantly enhanced drug delivery via inhalation (Nesamony et al., 2014; Pooladanda et al., 2021; Li et al., 2021). As compared to the corresponding traditional therapies, drug nanocarriers have typically offered distinct advantages, such as increased lung permeability, improved dissolution profiles, and superior biopharmaceutical properties (Gontijo et al., 2014).

In 1992, Cevc and Blume first described transferosomes as ultra-deformable, highly flexible vesicles consisting primarily of a permeation enhancer, in addition to the phospholipids (Cevc and Blume, 1992). Compared with traditional SLNPs, niosome and liposome transfersomes showed high elasticity, allowing them to squeeze themselves through different biological membranes. The deformability of transferosomes over liposomes was accredited to the permeation enhancer as it softened the lipid bilayers; they could squeeze between cells due to their elasticity, which improved the permeability (Salem et al., 2019a). In pulmonary therapy, transferosomal aerosols had the added benefit of facilitating uniform deposition of the locally active drugs into the lungs (Khan et al., 2020; Burton et al., 2015). Nebulizers provided the additional benefit of delivering transferosomes as aqueous dispersions without further processing as compared to the numerous available aerosol delivery systems (Elhissi et al., 2013). The stability of the aqueous dispersion of the transferosomes was then improved by using the lyophilization method and rehydrating the powder prior to nebulization (Guimarães et al., 2021).

The current study aimed to improve SA bioavailability and achieve direct lung targeting using a nebulized freeze-dried transferosomal formulation. The thin-film hydration method was used to prepare the SA-loaded transferosomes in a response-surface experimental study. First, the transferosome formulation was characterized for the encapsulation efficiency %, *in vitro* release, and size analysis, and then Design-Expert® was employed for the optimization. Finally, an optimized SA-transferosome was lyophilized into powder and adequately characterized. The optimized SA-transferosome was also examined for its SARS-CoV-2 antiviral activity before being tested for its *in vivo* pharmacokinetics. Moreover, to discover its broad anti-infective effect, SA and its optimized SA-transferosome were also screened against a panel of multidrug-resistant bacterial (*E. coli*, *P. aeruginosa*, *Salmonella typhimurium*, *Enterobacter* sp., *S. aureus*, *E. faecalis*, *S. mutans*) and fungal (*Aspergillus niger* and *Candida albicans)* pathogens.

2 Materials and methods

2.1 Materials

Sinapic acid, cholesterol, L-a phosphatidylcholine (soya lecithin), and lactose monohydrate were supplied by Sigma-Aldrich (St. Louis, MO). Tween 80 (polyoxyethylene sorbitan monooleate) of HLB = 15 and sodium deoxycholate (HLB = 16); cellophane membrane with a (12,000 kDa) molecular weight cut-off; methanol; HPLC-grade acetonitrile; and absolute ethanol were purchased from Fisher Scientific United Kingdom Ltd. (Loughborough Leicestershire, United Kingdom).

2.2 Formulation of SA-loaded transferosomes

Thin-film hydration was used to create SA-loaded transferosomes, with slight modifications identified by preliminary studies (Gamal et al., 2020). Briefly, absolute ethanol

TABLE 1 Factors and levels of user-defined response-surface design.

Factors	Levels		
	1	2	3
X_1: Ratio of cholesterol to phospholipid (w/w)	0:1	1:2	1:1
X_2: Surfactant type	Tween 80	Na-deoxy cholate	—
X_3: Ratio of phospholipid to surfactants (w/w)	75:25	85:15	—

was used to dissolve SA (10 mg), surfactant, cholesterol, lactose monohydrate (1,250 mg), and phosphatidylcholine. After that, the mixture was sonicated for 10 min and then moved into a round flask (100 mL). The absolute ethanol was evaporated in a vacuum employing a rotary evaporator (Stuart, United Kingdom) for 1 h at 40°C. Consequently, the obtained dried film was hydrated via 10 mL of an isotonic phosphate buffer (pH 7.4) for 1 h at 60°C. To transform the large vesicles into smaller ones, they were subjected to sonication for 20 min. After that, the developed protransferosomes were separated at 20,000 rpm for 3 h at 4°C in a cooling centrifuge (Hettich Zentrifugen, Germany), and then they were washed using isotonic phosphate buffer. The produced transferosomes were kept in tightly closed amber tubes at 4°C for further research.

2.3 Experimental design of SA-loaded protransferosomes

User-defined response-surface design was employed using Design-Expert software (version 10.0.0.3, United States) for the optimization procedure (Table 1). Twelve transferosomal formulations were developed (Table 2) using a ratio (w/w) of cholesterol to phospholipid (X1), surfactant type (X2), and the ratio of phospholipid to surfactants (X3) as independent variables. Consequently, the tested dependent variables were particle size (Y1), entrapment efficiency (Y2), and release percentage (Y3). Dependent and independent variables were selected according to literature review and preliminary studies.

2.4 Characterization of SA-loaded transferosomes

2.4.1 Size and zeta-potential study

A Malvern Zetasizer (Ver.7.11) determined the average transferosomal diameter via dynamic light scattering, Zeta potential, and size distribution curve. The formulated protransferosomes (1 mL) were diluted with isotonic buffer (up to 100 mL), and the analysis was replicated three times. The obtained findings are displayed in Table 2.

2.4.2 Characterization of SA entrapment efficiency percent

The entrapment percent of SA in transferosomes was assessed following the separation of the unentrapped SA in the supernatant obtained by several cooling centrifugation cycles at 4°C and 20,000 rpm for 3 h. First, the obtained vesicles were washed off the transferosomal vesicles. The isolated vesicles were then lysed by Triton X-100 in isotonic buffer (1% w/v), and the lysis was aided by consecutive heating cycles, up to 55°C before cooling to 25°C. After that, the obtained liquid was centrifuged for 20 min at 8,000 rpm to separate any debris (Salem et al., 2019b; Yusuf et al., 2017). Finally, the SA entrapment percentage was analyzed by UV-spectrophotometry at 322 nm, using isotonic phosphate buffer as the dilution media (Parmar et al., 2011).

TABLE 2 Composition and observed responses of different SA-loaded transferosome formulations.

Formulation code	X_1	X_2	X_3	Y_1 (nm) (mean ± SD)	Y2 (%) (mean ± SD)	Y3 (%) (mean ± SD)	Zeta potential (mV)
F1	1:1	Tween 80	85:15	380.43 ± 13.39	89.80 ± 2.65	19.74 ± 2.26	−28.1
F2	1:2	Na-deoxy cholate	85:15	221.87 ± 8.16	87.77 ± 1.70	25.65 ± 2.08	−29.3
F3	1:1	Na-deoxy cholate	75:25	298.57 ± 15.57	83.13 ± 3.55	29.36 ± 2.11	−42.1
F4	0:1	Na-deoxy cholate	85:15	198.33 ± 16.05	84.33 ± 2.97	34.91 ± 2.12	−31.2
F5	1:1	Tween 80	75:25	310.60 ± 11.59	76.28 ± 2.94	25.80 ± 2.07	−30.9
F6	1:1	Na-deoxy cholate	85:15	500.90 ± 9.27	89.53 ± 3.61	23.62 ± 2.22	−34.2
F7	0:1	Tween 80	75:25	195.67 ± 13.47	82.6 ± 3.25	47.47 ± 1.19	−29.1
F8	1:2	Tween 80	85:15	367.93 ± 12	89.23 ± 3.90	29.89 ± 2.03	−26.9
F9	1:2	Tween 80	75:25	255.63 ± 7.48	83.13 ± 2.24	37.87 ± 0.96	−28.3
F10	0:1	Na-deoxy cholate	75:25	141.7 ± 9.95	80.3 ± 2.69	42.84 ± 2.07	−30.9
F11	1:2	Na-deoxy cholate	75:25	204.20 ± 11.78	82.20 ± 1.90	31.35 ± 1.78	−32.7
F12	0:1	Tween 80	85:15	326.07 ± 9.98	87.87 ± 1.168	41.53 ± 2.11	−31.4

X1: ratio of cholesterol to phospholipid; X2: surfactant type; X3: ratio of phospholipid to surfactants; (Y1) particle size; (Y2) entrapment efficiency; (Y3) percentage of release; SD , standard deviation.

TABLE 3 Data of all dependent variables from regression analysis and analysis of variance.

Dependent variables	Model	F-value	*p*-value	Adjusted R^2	Predicted R^2	Adequate precision
Particle size	Quadratic	43.52	<0.0001	0.9285	0.9069	26.370
Entrapment efficiency	Quadratic	10.15	<0.0001	0.6467	0.5250	9.312
Percentage of release	Quadratic	18.96	<0.0001	0.9304	0.9085	27.085

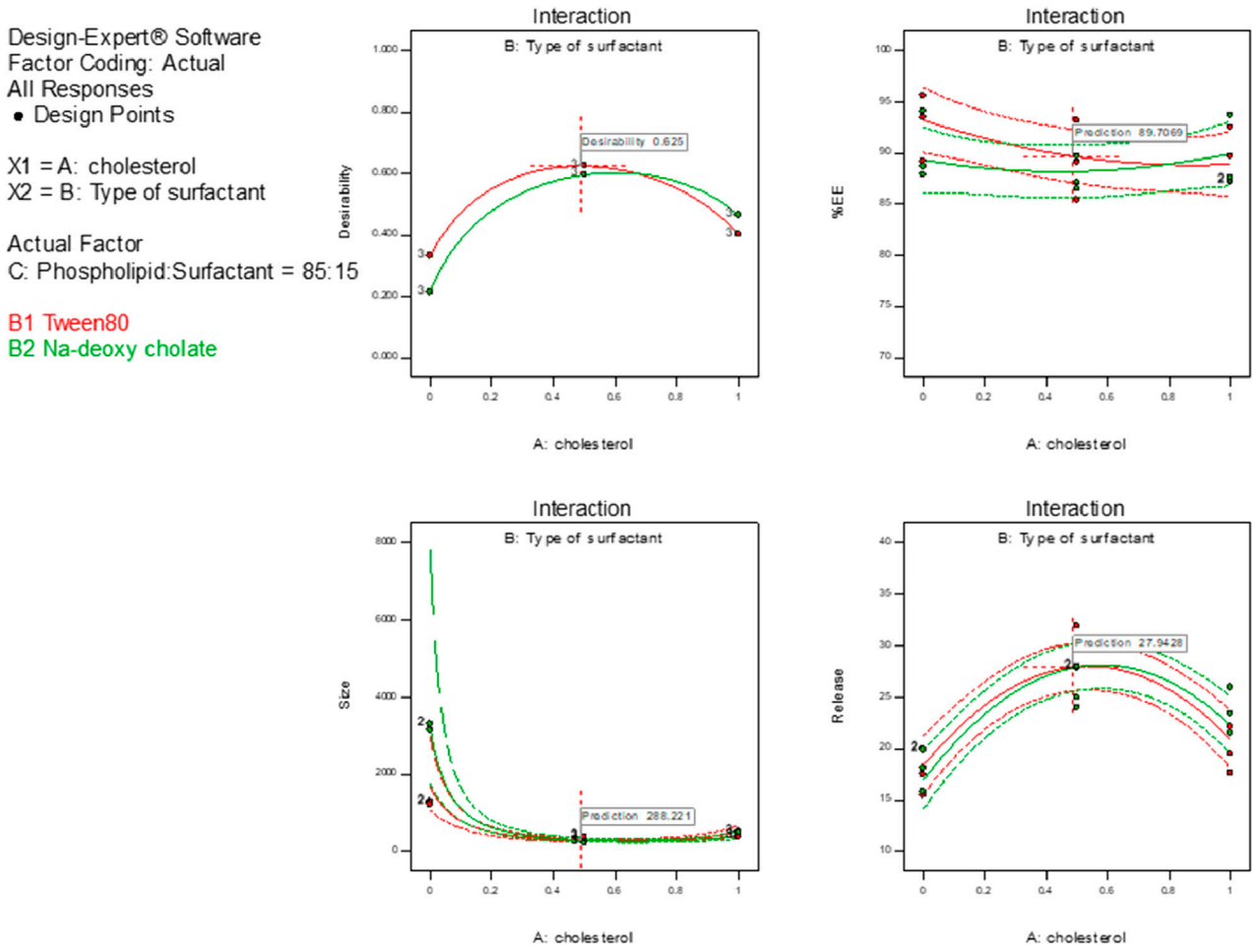

FIGURE 1
The impact of the independent variables on the responses.

2.4.3 *In vitro* SA release percent

The dialysis membrane method was utilized to determine the percentage of SA released from the developed transferosomes, using the USP-II dissolution apparatus (Jose et al., 2014; Salem et al., 2018). As the donor component, SA-loaded transferosomes entrapping 10 mg SA were added into an open-sided tube. One side of the tube was tightly enclosed via a 12,000 kDa-cellophane membrane, while the other was fixed to a paddle. The paddle stirring rate was 100 rpm at 37°C ± 0.50°C. The isotonic phosphate buffer was used as the receptor liquid (100 mL), and 10% propylene glycol was applied to maintain a sink environment (Aboud et al., 2016). Samples were withdrawn at various intervals (0.25, 0.5, 1, 2, 3, 4, 5, and 12 h) and substituted with similar volumes of isotonic phosphate buffer. The obtained samples were examined at 322 nm using a UV-spectrophotometer; the test was repeated thrice. The *in vitro* release percentage of SA was estimated by dividing the SA-entrapped quantity by the SA-released quantity and then multiplied by 100 (Salem et al., 2016). The percentage of SA released from the protransferosomes was estimated against the SA percentage released from the free SA suspension (10 mg). The optimized transferosomal formula was chosen according to the results of the characterization studies of the prepared SA transferosomes (Fatima et al., 2022).

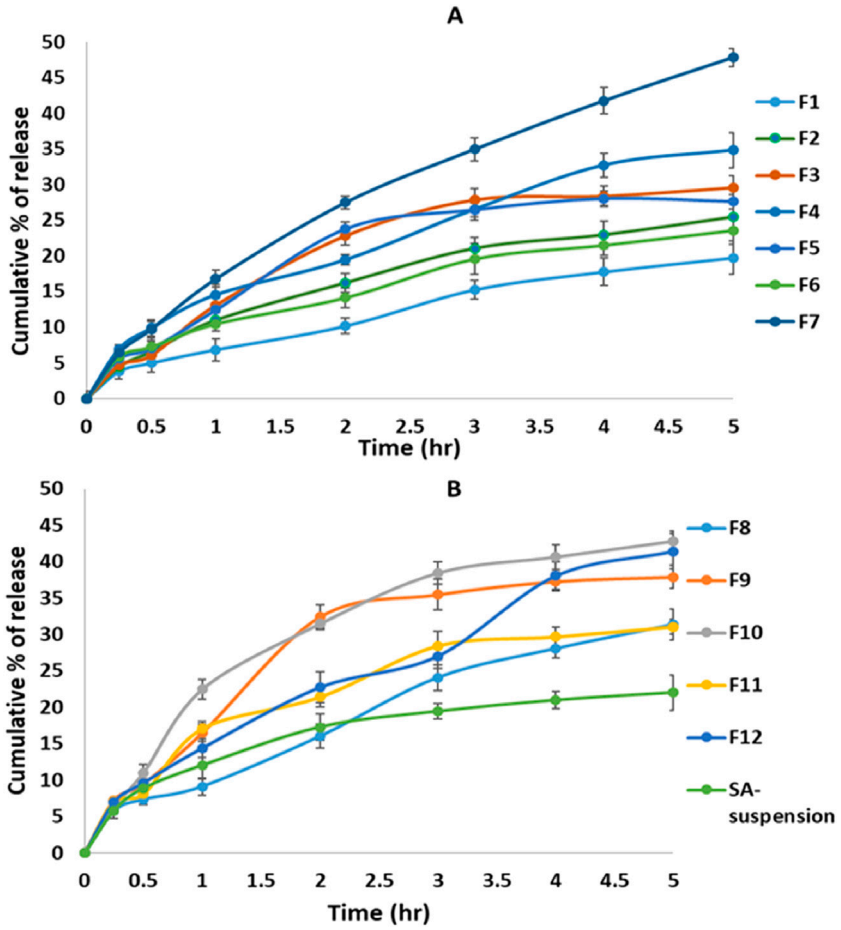

FIGURE 2
In vitro release profiles of sinapic acid from the prepared transferosomes: **(A)** F1–F7, **(B)** F8–F12 and SA suspension.

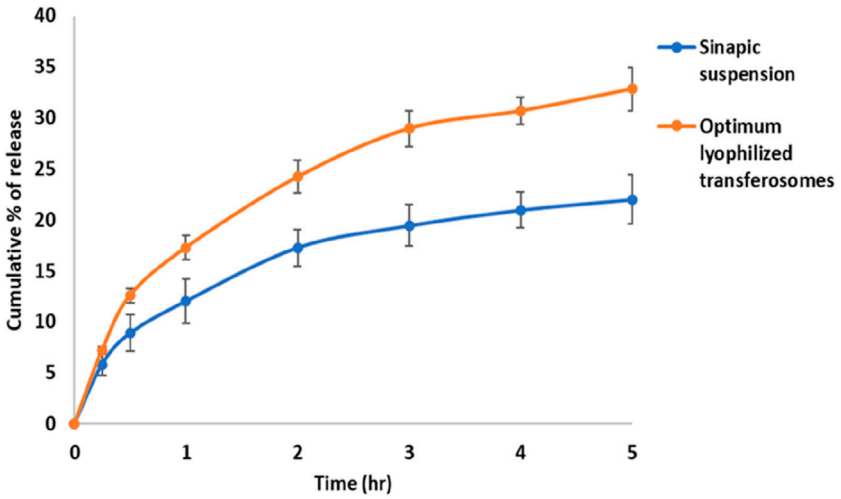

FIGURE 3
In vitro percentage of release of sinapic acid from optimal lyophilized transferosome and sinapic acid-suspension.

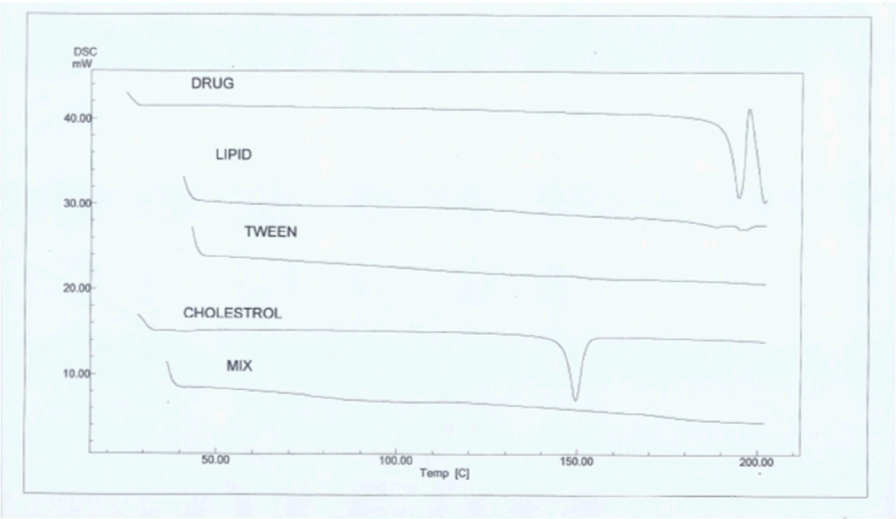

FIGURE 4
DSC thermograms of sinapic acid (drug), phospholipid, Tween 80, cholesterol, and the optimal transferosomes (mix).

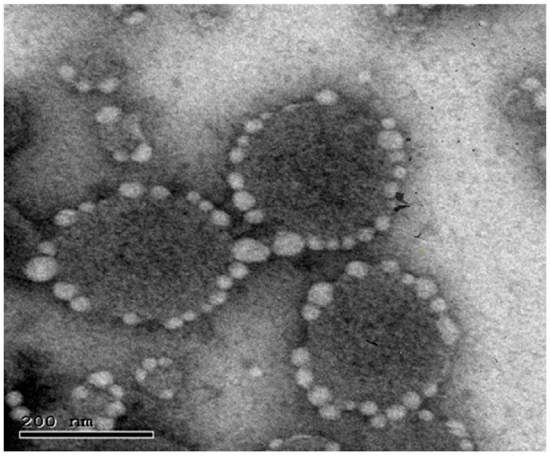

FIGURE 5
Photomicrograph of optimal lyophilized transferosomes using TEM.

2.5 Optimization of protransferosomes

The statistical significance obtained from the investigated data of each response was estimated using the ANOVA test at p-value < 0.05. The predicted and adjusted coefficients of determination (R2) were used to determine if the chosen model was suitable for the investigated data. The signal-to-noise ratio was determined using adequate precision to confirm that the applied model may well navigate the model's design spaces (Das et al., 2015). The optimization process also depended on using the highest desirability index (Gamal et al., 2020). The relationship between different factors and each response was explained according to the polynomial equations (Equations 1–3; Table 3).

$$1/\mathrm{Sqrt}\,(\mathrm{Size}) = +\,0.0040 - 0.0011X_1 + 0.00052X_2 - 0.00063X_3 - 0.00056X_1X_2 + 0.00026X_1X_3 + 6.09E - 6X_2X_3 - 7.01E - 5X_1^2 \quad (1)$$

$$\mathrm{EE\%} = 85.5833 + 0.46X_1 - 0.137X_2 + 3.41X_3 + 1.56X_1X_2 + 1.33X_1X_3 - 0.74X_2X_3 - 1.36X_1^2 \quad (2)$$

$$\mathrm{Release\%} = 31.19 - 8.53X_1 - 1.21X_2 - 3.28X_3 + 2.34X_1X_2 + 0.26X_1X_3 + 0.05X_2X_3 + 1.97X_1^2 \quad (3)$$

2.6 Formulation and characterization of the optimal SA protransferosomes

The optimized SA-loaded transferosomes were chosen based on the following criteria: maximizing the *in vitro* released SA, maximizing the EE%, and minimizing the mean particle size. Consequently, the selected optimized formula was developed using thin-film hydration, as previously described, and subjected to further characterization studies. As a result, the optimized transferosomes were prepared and analyzed for vesicle size, PDI, EE%, and % of SA released, as previously mentioned.

2.7 Preparation and characterization of the lyophilized, optimal SA protransferosomes

The optimal SA-protransferosomes were dried via freeze-dryer EF03 (Edwards High Vacuum, Ltd.) to develop protransferosomes powder. Then, the lyophilized optimal SA protransferosomes were applied to the following characterization studies.

2.7.1 Size analysis, drug content, and release study

The lyophilized powder of SA-protranferosomes was suspended in 100 mL isotonic phosphate buffer and then characterized for

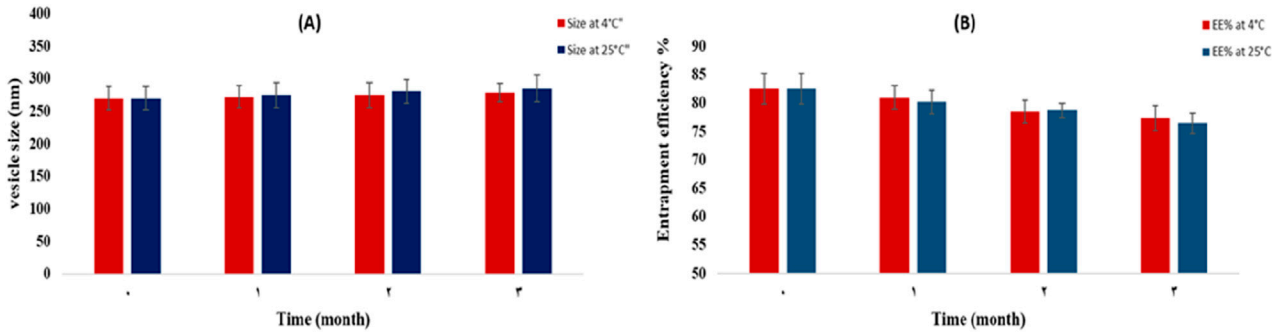

FIGURE 6
Effect of storage on the vesicle size **(A)** and EE% **(B)** of the optimal lyophilized protransferosomes, at 25°C and 4°C.

TABLE 4 Minimum inhibitory concentration (MIC) values (ug/mL).

Pathogen	MIC (μg/mL)			
	SA protransferosomes	SA	Ciprofloxacin	Nystatin
S. aureus ATCC 25923	2.05 ± 0.33	3.22 ± 0.15	0.5 ± 1.10	—
S. typhimurium ATCC 14028	1.13 ± 0.37	3.15 ± 1.07	0.12 ± 1.05	—
P. aeruginosa ATCC 90902	1.22 ± 0.42	7.23 ± 0.05	0.25 ± 0.05	—
E. coli O157 ATCC 700728	0.40 ± 0.09	2.23 ± 0.15	0.06 ± 1.17	—
E. faecalis	1.05 ± 1.09	—	0.5 ± 1.10	—
S. mutans	1.02 ± 0.85	—	0.8 ± 1.05	—
C. albicans	3.5.26 ± 0.14	6.5 ± 0.12	—	3.05 ± 0.18
A. niger	5.25 ± 0.15	6.23 ± 0.15	—	5.1 ± 0.25

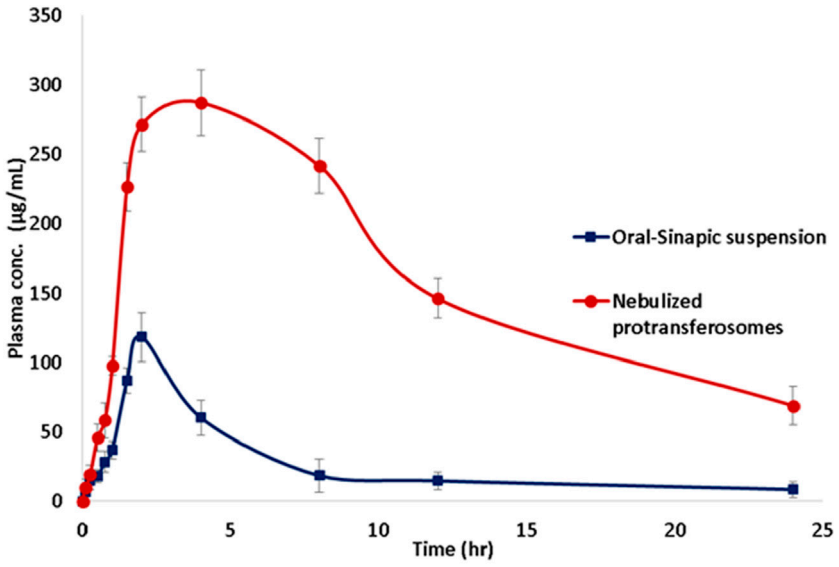

FIGURE 7
Mean sinapic acid concentrations in rabbit plasma after administration of oral sinapic suspension and nebulized lyophilized protransferosomes.

TABLE 5 Pharmacokinetic parameters for sinapic acid in rabbit plasma, following administration of oral sinapic suspension and nebulized protransferosomes.

Parameters	Oral sinapic suspension	Nebulized protransferosomes
C_{max} (μg/mL)	118.136	287.116
T_{max} (h)	2	4
AUC_{0-24} (μg.h/mL)	644.590	3930.165
$AUC_{0-\infty}$ (μg.h/mL)	746.686	4870.390
$MRT_{0-\infty}$ (h)	6.74	9.17
$t_{1/2}$ (h)	8.29	9.45

different parameters, including vesicular mean size, PDI, drug content, and % of SA released, as previously described.

2.7.2 Differential scanning calorimetry study (DSC)

The DSC study was carried out to clarify the thermal analysis of SA and the different components used in the developed transferosomes. The tested samples were placed on a standard crimped aluminum pan using an increased heating rate of 10°C per minute while the temperature was elevated from 25°C to 200°C (Bhattacharjee et al., 2017).

2.7.3 Morphology analysis

The optimized SA-loaded transferosome morphology was characterized via TEM-JEOL JEM-1400 transmission electron microscopy (Tokyo, Japan) through an 80 kV accelerating voltage. A grid of carbon copper was wrapped with a dried film of freshly developed protransferosomes. The protransferosomes were stained with a dye of phospho-tungstic acid, and the stained vesicles were dried; prior to this, the protransferosome morphologies were characterized via TEM (Fatima et al., 2022).

2.7.4 Stability study

After storing the optimized formula (equivalent to 5 mg SA) in firmly sealed amber glass tubes at 4°C and 25°C for 3 months, the optimized, lyophilized protransferosomes were tested for stability. Throughout the storage time, samples were taken and characterized for EE% and the protransferosome mean diameter, and stability testing was performed three times (Gupta and Trivedi, 2012).

2.7.5 Aerodynamic behavior of the optimized SA protransferosomes

The study was conducted according to the standard approach for aerodynamic testing outlined in Appendix XII F of the British Pharmacopoeia (Gamal et al., 2020). Briefly, samples of pure SA and the optimized SA protransferosomes (each equivalent to 200 mg) were individually packed into five size-3 hard gelatin capsules for aerodynamic testing. Before analysis, all components of the Andersen MKII Cascade Impactor were rinsed with methanol. The impactor was set up with a modified plate configuration—adjusted to a flow rate of 60 L/min using a vacuum pump—which required removing two stages (0 and 7) and adding two new plates at the top (stages 1 and 0). To prevent particle adhesion, all plates were pre-coated with silicone spray (Releasil B, Glamorgan, United Kingdom), and a GF 50 filter was placed at the base. Following pharmacopoeial guidelines, the pump was activated for 4 s per run, drawing 4 L of air through the impactor (Gamal et al., 2020). Each sample was tested five times using the Foradil™ Aerolizer inhaler. After drug dispersion, the deposited particles on each stage and filter were collected by soaking them in 10% methanol and sonicating them for 3 min. The aerodynamic performance was analyzed using Copley Scientific's CITDAS software (United Kingdom) to determine three key parameters: fine particle fraction (FPF%), fine particle dose (FPD, μg), and mass median aerodynamic diameter (MMAD, μm) (Gamal et al., 2020). MMAD plays a crucial role in determining where inhaled particles will deposit in the respiratory tract, while FPF was calculated as the percentage of drug particles that exited the mouthpiece relative to the total amount collected in the throat piece and all impactor stages.

2.8 In vitro antibacterial, antifungal, and antiviral activity studies

2.8.1 Antibacterial activity

To measure the antibacterial activity of the tested compound against Gram-negative (*E. coli* 0157 ATCC700728, *P. aeruginosa* ATCC90902, *S. typhimurium* ATCC14028, *Enterobacter* sp.) and Gram-positive (*S. aureus* ATCC25923, *E. faecalis*, *S. mutans*), and acid-fast bacteria *Mycobacterium* sp., the method described by Alhadrami et al. (2021) was used (Alhadrami et al., 2020). The test was performed in 96-well flat polystyrene plates. Ten microliters of tested SA or SA-protranferosomes (final concentration of 250 μg/mL) was added to 80 μL of lysogeny broth (LB broth). Afterward, each bacterial suspension was adjusted to a final concentration of 100 cfu/mL (OD600 nm), and 10 μL of the bacterial culture suspension was then added to the sample preparation of SA or SA-protranferosomes in LB. The plates were incubated overnight at 37°C. After incubation, the positive antibacterial effect of the tested compound was observed as clearance in the wells. For compounds without antibacterial activity, the growth media appeared opaque in the wells. The control consisted of the pathogen without any treatment. The absorbance was measured after approximately 20 h at OD600 using a Spectrostar Nano Microplate Reader (BMG LABTECH GmbH, Allmendgrun, Germany).

2.8.2 Antifungal activity

For pathogenic fungi, the activity of the tested SA or SA-protranferosomes was determined against *A. niger* and *C. albicans*, obtained from Microbial chemistry culture collection,

National Research Center, Egypt, using a microplate assay (MTP) with Sabouraud Dextrose Broth (SDB), according to Pierce et al. (2010) with some modification (Pierce et al., 2010). After 48 h of incubation at 30°C in potato dextrose broth (PDB), the fungal cells were recovered after centrifugation and washed twice with sterile PBS. The cells were counted using a hemocytometer and adjusted to a final concentration of 1.0×10^6 cells/mL. PDB (180 µL) was added into wells of a microtiter plate, followed by the addition of 10 µL of the test molecule (final concentration of 250 µg/mL) and 10 µL of an overnight fungal seed. After incubation, the positive antifungal effect of the tested compound was observed as clearance in the wells. Compounds without antifungal activity resulted in opaque growth media in the wells. The control consisted of the non-treated fungal pathogen. The absorbance was measured after approximately 20 h at OD_{600} using a Spectrostar Nano Microplate Reader (BMG LABTECH GmbH, Allmendgrun, Germany).

2.8.3 Minimum inhibitory concentration (MIC)

The minimum inhibitory concentration (MIC) of the evaluated drug against pathogenic strains was determined using a microplate experiment and serial dilution technique. A stock solution of the antimicrobial compound was prepared by dissolving it in a suitable solvent, such as dimethyl sulfoxide (DMSO) or water, to achieve the necessary concentration. The pathogens, comprising both Gram-negative and Gram-positive bacteria, were cultivated in Mueller–Hinton Broth (MHB) for each strain. Serial two-fold dilutions of the compound were prepared on a 96-well microtiter plate, starting with a high concentration in the first column and progressively decreasing in subsequent columns. Each well was inoculated with an identical amount of the bacterial suspension, calibrated to a standard inoculum density (typically 10^5 CFU/mL), and the plate was incubated at 37°C for 18–24 h. After incubation, the MIC was determined by visually examining the wells for bacterial growth. The absence of turbidity indicated inhibition of growth. The OD_{600} was measured using a microplate reader. The minimum concentration of the compound that prevented observable growth was designated as the MIC. This assay provides an accurate assessment of the antibacterial efficacy of the compound against each evaluated pathogen. In the same way, MIC for fungi was determined using the same technique with potato dextrose broth and incubation at 30°C for 48 h.

2.8.4 Antiviral analysis

Vero E6 cells (ATCC® number 1568) were maintained and grown in Dulbecco's modified Eagle medium (DMEM) containing 10% fetal bovine serum (FBS) as described before (Al-Amri et al., 2017). SARS-CoV-2/human/SAU/85791C/2020 (Gene accession number MT630432.1) was isolated from a human nasopharyngeal swab confirmed positive by RT-PCR in August 2020. IRP number H-02-K-076-00520-298 was obtained from the Saudi Ministry of Health to use patient samples. All experiments involving live SARS-CoV-2 were performed following the internationally recommended safety measures and precautions in the Biosafety Level 3 Facility at the Special Infectious Agent Unit, King Fahd Medical Research Center, King Abdulaziz University, Saudi Arabia. The cytotoxicity and antiviral activities were investigated using Vero E6 cells (Sigma Aldrich). Then, serial concentrations of the test compounds incubated with Vero E6 were infected with SARS-CoV-2 (SARS-CoV-2/human/SAU/85791C/2020 isolate) at a multiplicity of infection (MOI) of approximately 0.5. DMSO was used as a solvent control. The detailed procedure of the quantitative real-time PCR antiviral assay can be found in the Supplementary Material.

2.8.5 Cellular proliferation and cytotoxicity assays

A directly automated cell-counting method was utilized to determine the cell proliferation. At first, the counted cells were seeded on CellCarier-96-optical plates (PerkinElmer) before the study, followed by the addition of SA or remdesivir, and finally, they were incubated for 3 days. Next, the cells were counted via a PerkinElmer EnSight reader. Finally, the counted number of cells was compared with those obtained in the solvent controls.

2.8.6 Quantification of RNA

The viral content in harvested cellular supernatants (125 µL) was deactivated via MagNA Pure LC total NA Lysis/binding buffer. Then, the viral RNA isolation was performed via the isolation device of MagNA Pure 24 NA, consistent with Roche's guidelines. The amplification was performed via a Master Probe kit for RNA, consistent with Roche's guidelines. All PCRs and quantifications were performed via Roche's guidelines with the respective cycler software.

2.9 *In vivo* pharmacokinetics study

The *in vivo* performance of the optimal formulation was examined utilizing *in vivo* pharmacokinetic examination. In addition, the bioavailability of SA was studied in a rabbit model following nebulization of the re-dispersed optimal lyophilized SA protransferosomes and oral administration of the SA suspension.

A total of 12 adult albino rabbits weighing 1.35–1.60 kg were distributed into two groups. Group 1 received 10 mg of the SA suspension orally with the help of a gauge needle (Günther et al., 2004). In comparison, group 2 received a suspension of the optimized lyophilized protransferosomes (10 mg of SA) through nebulization after anesthesia using diethyl ether (Gamal et al., 2020; Pastor et al., 2015). The protocol developed for this *in vivo* experiment was certified through the Animal Ethics Committee of Nahda University. (Regd. No. NUB-032-022). Blood samples were taken using EDTA tubes at various intervals for 24 h; then, they were centrifuged for 10 min at 5,000 rpm, and then plasma separation and HPLC-UV analysis were performed.

The plasma samples were analyzed using Dionex Ultimate 3000 UHPLC, supplied with an auto-sampler, a diode array detector (Massachusetts, United States), and a quaternary solvent delivery pump. The C18 reverse-phase column ZORBAX Eclipse Plus® (5 µm, 250 × 4.6 mm) (California, United States) was used for the development and quantitation. The internal standard was ciprofloxacin, while the mobile phase was water–acetonitrile (2: 98% v/v) at a 1.0 mL/min flow rate. The test temperature was set to 25°C, and UV detection was carried out at 320 nm. The output signal was checked and processed using Chromeleon software. Different pharmacokinetic parameters, such as MRT, AUC, $t_{1/2}$, T_{max}, and C_{max}, were computed via the PKSolver program. The statistical data analysis utilized SPSS 16.0 software (Chicago, IL).

3 Results and discussion

3.1 Optimization of protransferosomes and experimental model evaluation

The user-defined design was a proper statistical design-of-experiments (DOE) technique, and it was used to perform the optimization process. DOE was utilized for this study to estimate the model parameters because it lowered the variance of the constraints estimator due to its efficient norm reduction of the covariance matrix. In addition, it was suggested that applying a DOE design would lead to fewer samples being needed, as compared to other designs, while not impacting the estimated error and variance, which was strongly desired (Ali et al., 2021).

Twelve transferosomes were developed corresponding to the user-defined experimental design, and then they were characterized for numerous responses. In addition, the interactions among the examined independent and dependent variables were demonstrated mathematically using polynomial equations (Equations 1–3; Table 3).

The quadratic approach was observed as the best-fitting model for the Y1, Y2, and Y3 variables. All the obtained models were significant at a *p*-value of 0.05. The positive coefficient for the impact of each factor on the measured responses was considered synergistic, while the antagonistic influence was determined by a negative coefficient (Salem et al., 2019a). All the responses indicated good agreement between the predicted R2 of the determination and the adjusted R2.

Given that the applied model's signal-to-noise ratio had a sufficient degree of precision, that is, more significant than 4, it could be used to explore the design space (Table 3; El-Menshawe et al., 2018). A response-surface analysis was performed to explain how certain independent variables had affected the observed responses. It was clear from the resulting equations (Table 3) that the intercept had a positive influence on each of the three responses. Figure 1 shows how the independent variables affected the measured responses.

3.2 Effect of design variables on vesicle size (Y1)

The ANOVA test results showed that each of the tested factors significantly affected the vesicle size at a *p*-value < 0.05, except X2. The size of the transferosomes varied from 141.7 ± 9.95 to 500.90 ± 9.27 nm (Table 2). The examined factors (X1 and X3) had an antagonistic influence on the transferosome mean size, excluding X2, which had a synergistic impact. The increase in the concentration of phospholipid or cholesterol resulted in a significant increase in the transferosome size, while the increase in the surfactant concentration significantly decreased the transferosome size (Khan et al., 2020).

Our results agreed with those of Moawad et al. (2017) as we found that the Tween 80 (HLB = 15) samples showed smaller transferosomes, as compared to the sodium deoxycholate samples (HLB = 16). Despite the higher HLB of sodium deoxycholate, the samples showed larger vesicular sizes, explained by their anionic character. This resulted in a negative charge and caused a powerful repulsion force to develop among the lamellae of the vesicles. Consequently, the aqueous core size increased, producing larger vesicles, as previously mentioned (Moawad et al., 2017). The homogeneity of the vesicular dispersions was assessed using the PDI. A system with a PDI of 0 had mono-dispersed vesicles, whereas a system with a PDI of 1 had high poly-dispersed vesicles (Song et al., 2022). The obtained PDI of the SA-loaded transferosomes ranged from 0.103 ± 0.06 to 1.00 ± 0.25, indicating that some transferosomes had a balanced size distribution and homogeneity (Table 2).

The zeta potential (ZP) is regarded as an essential measure of the physical stability of nano-formulations. The high repelling forces between the vesicles and the large ZP on the surfaces (positive or negative) minimized the aggregation of the vesicles and provided more sustained vesicular stability. The transferosome stability resulted from the decreased interfacial tension caused by using a high surfactant concentration. In addition, the prepared transferosomes had a negative charge ranging from −18.1 to −42.1 mV (Table 2). This high negative charge caused steric stabilization and electrostatic repulsion (Salem et al., 2019c). Nanoparticles have been demonstrated to have a stronger affinity for biological membranes due to the predominant electrostatic interactions. The uptake of strongly negatively charged nanoparticles was preferred by the cells despite the presence of extensive negative charges in the biological membranes due to the predominance of the non-specific interaction mechanisms, as well as the cluster arrangement of the nanoparticles (Salem et al., 2019c).

3.3 Effect of design variables on EE% (Y2)

The ANOVA results indicated that each of the tested factors significantly affected the EE% at a *p*-value < 0.05, except X2. As shown in Table 2, the entrapment efficiency of the transferosomes varied from 76.28% ± 2.94% to 89.53% ± 3.61%. The high SA entrapment tendency may have been caused by the hydrophobicity of SA, which made it insoluble in water (Shakeel et al., 2016a).

The investigated variables (X1 and X3) revealed synergistic interactions, as compared to variable X2, which displayed a significant negative interaction. It was evident that SA entrapment had been increased by the higher ratio of phospholipids to surfactants. These results could have been related to the liquid membrane rupture caused by the high surfactant concentration, which weakened the membrane entrapping the SA (López et al., 1998). Consequently, the increase in surfactant concentration showed a decline in EE%.

Regardless of the kind of surfactant, the percentage of entrapped SA increased with higher cholesterol-to-phospholipid ratio. The transferosomal membrane became highly rigid, and the spaces between the phospholipid and surfactant molecules were filled with cholesterol. This reduced the drug leakage from the vesicles through the cholesterol interaction with the membrane core during the annealing process. Accordingly, the capacity of the transferosomal bilayer membrane to entrap hydrophobic drugs was increased; this might also have been due to the phospholipid bilayer conversion to the solid-phase bilayer as a result of the inclusion of cholesterol (Gyanewali et al., 2021; Khan et al., 2021).

3.4 Effect of design variables on *in vitro* release (Y3)

The ANOVA results showed that each tested factor significantly affected the SA release at p-value < 0.05. The examined factors X1, X2, and X3 had a significant antagonistic impact on the release percentage.

As shown in Figure 2, the examined release varied from 19.74% ± 2.26% to 47.47% ± 1.19%. The increase in the ratio of phospholipid to cholesterol resulted in a significant decrease in the SA released. In contrast, the increase in surfactant concentration significantly increased SA release, owing to the added rigidity and the hydrophobicity of the prepared transferosomes caused by the cholesterol (Abd-Elbary et al., 2008). Using Tween 80 as a surfactant significantly increased SA release, as compared to use of sodium deoxycholate. These findings agreed with those of both Moawad et al. (2017) and Jain et al. (2003).

3.5 Selection of optimized SA protransferosomes

The optimization process for the prepared transferosomes aimed to identify the levels of the independent variables required to develop the transferosomes with optimal characteristics. The numerical optimization of the Design-Expert® program was utilized to select an optimal formulation from 12 prepared transferosomal formulations in compliance with the DOE design. The following optimization criteria were used: (i) achievement of maximum percentage of *in vitro* release; (ii) maximum percentage of entrapment efficiency; (iii) minimal size of transferosomes. Following the numerical optimization, the formulation composed of Tween 80 as a surfactant (85:15% w/w as a ratio of phospholipid to Tween 80) and 1:2 w/w as a ratio of cholesterol to phospholipid was selected as the optimized SA-loaded transferosomes. The developed optimized formulation showed a desirability index of 0.678, an *in vitro* release of 28.03% ± 2.3%, an EE of 89.47% ± 3.01%, and a mean vesicle size of 232.13 ± 3.30. The observed study and predicted model achieved an acceptable level of agreement, proving the validity of the model.

3.6 Characterization of the lyophilized optimal SA protransferosomes

The re-dispersed lyophilized protransferosomes had a vesicle size of 270.2 ± 5.1 nm and a drug content of 98.11% ± 3.6%. The *in vitro* percentage of the release of SA from the optimal lyophilized transferosome was 32.8% ± 2.1%, as displayed in Figure 3.

3.6.1 Differential scanning calorimetric analysis (DSC)

The melting parameters and DSC thermograms for the phospholipid, Tween 80, cholesterol, SA, and SA-loaded protransferosomes are shown in Figure 4. The DSC thermograms displayed 2 endothermic peaks that appeared at 188°C and 194°C, corresponding to the melting temperature of the phospholipids with enthalpy fusion ΔH = − 10.6 and −0.8 MJ, respectively. In addition, two endothermic peaks appeared at 148°C and 167°C, corresponding to the melting temperature of the Tween 80 with enthalpy fusion ΔH = − 10.6 and −2.8 MJ, respectively. Additionally, two endothermic peaks appeared at 150°C and 170°C, corresponding to the melting temperature of the lactose with enthalpy fusion ΔH = − 318.2 and −77.9 MJ, respectively. The DSC thermograms displayed an endothermic peak at 149°C, indicating the melting temperature of the cholesterol with enthalpy fusion ΔH = −199.8 mJ. In comparison, the sharp endothermic peaks of SA were observed at 194°C, with enthalpy fusion ΔH = −303.0 mJ. The SA-loaded protransferosomes exhibited two endothermic peaks at 145°C and 170°C, with enthalpy fusion ΔH = − 386.7 and −40.2 mJ, correspondingly. The crystallinity of the phospholipid, cholesterol, Tween 80, and lactose samples was reduced after mixing as they assembled as a transferosome bilayer. The crystallinity of SA was reduced upon loading the transferosomes as SA was loaded within the vesicles in an amorphous form. Moreover, including surfactants in the formulations may have contributed to the crystal distortion and, in turn, a depression in the melting points (Dolatabadi et al., 2021).

3.6.2 Morphology analysis of optimal protransferosomes

The response-surface morphological analysis of the optimal protransferosomes by TEM is displayed in Figure 5. The photomicrograph presented the prepared protransferosomes as well-identified, homogenous, spherical nano-vesicles. In addition, the TEM photomicrograph showed the coating of the carrier particles on the transferosome surface, which was observed as bright spots.

3.6.3 Stability study

The stability study of the optimized SA protransferosomes at 4°C and 25°C, after 1, 2, and 3 months, was evaluated by studying the EE % and vesicle size. As displayed in Figure 6, the EE % decreased insignificantly during the 3 months of the study. In addition, the vesicle size increased insignificantly at a p-value > 0.05, after applying the ANOVA test. The vesicle tendency to coalesce due to the weak cohesive and van der Waals forces, which were present all over the transferosomes, had been reported as the cause of the increase in the transferosome size (Gamal et al., 2020).

3.6.4 Aerodynamic behavior of the optimized SA protransferosomes

The cascade impactor was used to evaluate and compare the aerodynamic properties of the optimized protransferosome powder and pure SA. Statistical analysis revealed that the protransferosome formulation outperformed that of pure SA in all tested parameters (*p* < 0.05). Fine particle fraction (FPF) obtained for optimized protransferosome powder achieved 29.85% ± 5.8% FPF, significantly higher ($p < 0.05$) than that of pure SA (17.79% ± 2.33%). Similarly, fine particle dose (FPD) obtained for optimized protransferosomes exhibited markedly greater FPD values. Particle size emerged as a key reason governing respiratory tract deposition patterns, which directly influence both the deposition site and the delivered drug amount within the lungs (Gamal et al., 2020; Salem et al., 2011). The results also showed that the optimized protransferosomes demonstrated significantly smaller MMAD values (2.96 ±

0.41 μm) than pure SA (3.86 ± 0.10 μm) ($p < 0.05$), indicating superior aerosol performance. This enhanced aerodynamic behavior may be due to the improved powder flow characteristics of the protransferosomes, which may explain the more efficient lung targeting compared to the unformulated SA.

3.7 *In vitro* antibacterial and antifungal activity study

Both SA and its protransferosomes demonstrated good inhibition for most of the bacterial and fungal pathogens tested (Table 4). MIC for the antibacterial activity demonstrated enhanced activity of SA protransferosomes compared to the pure SA, moving it much closer to the positive control (Table 4). Interestingly, in the case of *E. faecalis* and *S. mutans*, although the pure SA did not show good activity, SA protransferosomes demonstrated comparable effects to ciprofloxacin, the positive control. Additionally, SA protransferosomes demonstrated comparable MIC to nystatin, the positive antifungal control drug, against both *C. albicans* and *A. niger* (Table 4) and a more enhanced effect compared to pure SA.

Phenolic compounds such as SA can exhibit varying antibacterial activity against different bacterial pathogens due to differences in cell envelope composition, permeability, and resistance mechanisms. For example, Gram-negative bacteria possess an outer membrane that can hinder the penetration of phenolics, reducing their efficacy, while Gram-positive bacteria lack this barrier, making them more susceptible. Additionally, variations in membrane-bound enzymes, efflux pumps, and intracellular targets influence how each strain responds to phenolic stress. The compound's activity may also depend on its ability to disrupt membrane integrity, generate oxidative stress, or denature proteins, mechanisms that can vary in effectiveness depending on the bacterial species and strain.

The higher MIC of SA protransferosomes vs. ciprofloxacin reflects its superior potency, while the lower MIC vs. free SA highlighted the benefits of transfersomes in improving the activity compared to the pure SA, due to its ultra-deformability that enhances penetration through biological membranes due to their elasticity. Transferosomes retain SA longer, so they provide prolonged release, which sustains its activity longer. It also provides a shield for SA from enzymatic degradation through encapsulation. These properties regarding transfersomes may be the explanation for its enhanced activity (Aguilar-Toalá et al., 2022; Opatha et al., 2020).

3.8 *In vitro* antiviral activity study

An *in vitro* antiviral assay of SA against SARS-CoV-2 showed an IC_{50} value of 2.29 ± 0.065 μg/mL. This value was comparable to our previous report, where IC_{50} had been found to be 2.69 μg/mL (Orfali et al., 2021). The IC_{50} of the reference antiviral drug, remdesivir, was 0.036 ± 0.002 μg/mL. Both SA and remdesivir showed significantly low cytotoxicity to the host cells, with a CC_{50} of 188.33 ± 10.8 and 170.74 μg/mL, respectively.

The newly formulated SA protransferosomes showed significantly enhanced antiviral activity: 50% viral growth inhibition at significantly reduced concentrations (IC_{50} = 0.016 ± 0.008 μg/mL; the IC_{50} of the lyophilized SA formulation = 0.0179 ± 0.0089 μg/mL). Hence, this new formulation was more potent than remdesivir. Accordingly, the present nano-formulation improved the cellular delivery of SA.

The enhanced antiviral activity of SA-loaded protransferosomes can be attributed to the unique physicochemical properties of transferosomes, particularly their ultra-deformability. This high flexibility allows transferosomes to traverse biological barriers more effectively than conventional liposomes by squeezing through tight intercellular spaces and facilitating fusion with cellular membranes, thereby improving intracellular delivery and bioavailability of SA (Elsayed et al., 2006; Gupta et al., 2005). Additionally, transferosomes offer a sustained release profile, prolonging the retention and therapeutic effect of SA (Song et al., 2012). The encapsulation also protects SA from enzymatic degradation, preserving its structural integrity and antiviral efficacy (Aguilar-Toalá et al., 2022; Opatha et al., 2020). These combined features likely contribute to the superior antiviral performance observed with SA protransferosomes. Of course, this should be supported by future *in vivo* studies.

3.9 *In vivo* pharmacokinetic study

Each of the calculated pharmacokinetic parameters was determined by constructing a plasma–concentration time curve, as presented in Figure 7. The relative bioavailability of the nebulized SA protransferosomes was 6.1-fold of the oral SA. The AUC for the SA protransferosomes was significantly more than the AUC of the oral SA, by a factor of 6.1 ($p = 0.001$). The increased bioavailability of the SA protransferosomes can be attributed to their ability to bypass the first-pass hepatic processing. Whereas the oral SA had a T_{max} of 2 h and a C_{max} of 118.136 μg/mL, the SA protransferosomes had a T_{max} of 4 h and a C_{max} of 287.116 μg/mL, as shown in Table 5. Moreover, the SA protransferosomes had an increased MRT and t1/2 with a considerable ($p = 0.001$) increase and effectively maintained their plasma concentration. The longer T_{max}, which was correlated with the release date, may have been caused by the prolonged SA release into the alveolar fluid from the protransferosomes before it could be absorbed via the systemic circulation (Gamal et al., 2020; Saimi et al., 2021).

4 Conclusion

This study focused on developing a nanocarrier that could deliver SA to the lungs. The developed SA protransferosomes displayed dramatically improved bioavailability and *in vitro* antiviral efficacy through pulmonary nebulization, making them a potential SA delivery strategy. Additionally, the developed SA protransferosomes showed enhanced antibacterial and antifungal effects against a panel of tested pathogens. As a result, the produced SA protransferosomes could be considered a safe and efficient pulmonary targeting system via nebulization. Furthermore, there are encouraging prospects for the therapeutic use of medications that target the lungs, which could be crucial therapies for many other pulmonary disorders, SARS-CoV-2 infection, and bacterial and

fungal infections. The current study should be verified using a suitable animal model to quantify the lung targeting efficiency and safety.

Data availability statement

The original contributions presented in the study are included in the article/Supplementary Material; further inquiries can be directed to the corresponding author.

Ethics statement

The animal study was approved by the Animal Ethics Committee of Nahda University. The study was conducted in accordance with the local legislation and institutional requirements.

Author contributions

HA: software, project administration, writing – original draft, funding acquisition, methodology, and investigation. AG: investigation, writing – original draft, software, methodology, and formal analysis. NA: investigation, writing – review and editing, methodology, and formal analysis. AS: writing – original draft, methodology, formal analysis, validation, software, and investigation. MR: project administration, supervision, funding acquisition, validation, data curation, conceptualization, resources, and writing – review and editing. DN: software, supervision, resources, conceptualization, formal analysis, validation, methodology, and writing – original draft.

Funding

The author(s) declare that financial support was received for the research and/or publication of this article. This study was funded by the British Council, UK-Saudi Challenge Fund 2023-24 – UWS/KAU.

Acknowledgments

The authors therefore acknowledge with thanks the British Council for their financial and technical support.

Conflict of interest

The authors declare that the research was conducted in the absence of any commercial or financial relationships that could be construed as a potential conflict of interest.

Generative AI statement

The author(s) declare that no Generative AI was used in the creation of this manuscript.

Publisher's note

All claims expressed in this article are solely those of the authors and do not necessarily represent those of their affiliated organizations, or those of the publisher, the editors and the reviewers. Any product that may be evaluated in this article, or claim that may be made by its manufacturer, is not guaranteed or endorsed by the publisher.

Supplementary material

The Supplementary Material for this article can be found online at: https://www.frontiersin.org/articles/10.3389/fnano.2025.1599272/full#supplementary-material

References

Abd-Elbary, A., El-laithy, H. M., and Tadros, M. I. (2008). Sucrose stearate-based proniosome-derived niosomes for the nebulisable delivery of cromolyn sodium. *Int. J. Pharm.* 357 (1–2), 189–198. doi:10.1016/j.ijpharm.2008.01.056

Aboud, H. M., Ali, A. A., El-menshawe, S. F., and Elbary, A. A. (2016). Nanotransfersomes of carvedilol for intranasal delivery: formulation, characterization and *in vivo* evaluation. *Drug Deliv.* 23 (7), 2471–2481. doi:10.3109/10717544.2015.1013587

Adamson, C. S., Chibale, K., Goss, R. J. M., Jaspars, M., Newman, D. J., and Dorrington, R. A. (2021). Antiviral drug discovery: preparing for the next pandemic. *Chem. Soc. Rev.* 50 (6), 3647–3655. doi:10.1039/d0cs01118e

Aguilar-Toalá, J. E., Quintanar-Guerrero, D., Liceaga, A. M., and Zambrano-Zaragoza, M. L. (2022). Encapsulation of bioactive peptides: a strategy to improve the stability, protect the nutraceutical bioactivity and support their food applications. *RSC Adv.* 12 (11), 6449–6458. doi:10.1039/d1ra08590e

Al-Amri, S. S., Abbas, A. T., Siddiq, L. A., Alghamdi, A., Sanki, M. A., Al-Muhanna, M. K., et al. (2017). Immunogenicity of candidate MERS-CoV DNA vaccines based on the spike protein. *Sci. Rep.* 7, 44875. doi:10.1038/srep44875

Alhadrami, H. A., Hamed, A. A., Hassan, H. M., Belbahri, L., Rateb, M. E., and Sayed, A. M. (2020). Flavonoids as potential anti-MRSA agents through modulation of PBP2a: a computational and experimental study. *Antibiot. (Basel)* 9 (9), 562. doi:10.3390/antibiotics9090562

Ali, A. A., Hassan, A. H., Eissa, E. M., and Aboud, H. M. (2021). Response surface optimization of ultra-elastic nanovesicles loaded with deflazacort tailored for transdermal delivery: accentuated bioavailability and anti-inflammatory efficacy. *Int. J. Nanomedicine* 16, 591–607. doi:10.2147/ijn.s276330

Angourani, H. R., Zarei, A., Moghadam, M. M., Ramazani, A., and Mastinu, A. (2023). Investigation on the essential oils of the Achillea species: from chemical analysis to the *in silico* uptake against SARS-CoV-2 main protease. *Life* 13 (2), 378. doi:10.3390/life13020378

Antimicrobial Resistance Collaborators, Ikuta, K. S., Sharara, F., Swetschinski, L., Robles Aguilar, G., Gray, A., et al. (2022). Global burden of bacterial antimicrobial resistance in 2019: a systematic analysis. *Lancet* 399 (10325), 629–655. doi:10.1016/S0140-6736(21)02724-0

Balagangadharan, K., Trivedi, R., Vairamani, M., and Selvamurugan, N. (2019). Sinapic acid-loaded chitosan nanoparticles in polycaprolactone electrospun fibers for bone regeneration *in vitro* and *in vivo*. *Carbohydr. Polym.* 216, 1–16. doi:10.1016/j.carbpol.2019.04.002

Bhattacharjee, A., Verma, S., Ranjan, P., Verma, P., Singh, S. K., and Chakraborty, A. (2017). Fabrication of liquid and solid self-double emulsifying drug delivery system of atenolol by response surface methodology. *J. Drug Deliv. Sci. Technol.* 41, 45–57. doi:10.1016/j.jddst.2017.06.014

Burton, A. J., Giguère, S., and Arnold, R. D. (2015). Pharmacokinetics, pulmonary disposition and tolerability of liposomal gentamicin and free gentamicin in foals. *Equine Vet. J.* 47 (4), 467–472. doi:10.1111/evj.12309

Cevc, G., and Blume, G. (1992). Lipid vesicles penetrate into intact skin owing to the transdermal osmotic gradients and hydration force. *BBA - Biomembr.* 1104 (1), 226–232. doi:10.1016/0005-2736(92)90154-e

Das, S. K., Yuvaraja, K., Khanam, J., and Nanda, A. (2015). Formulation development and statistical optimization of ibuprofen-loaded polymethacrylate microspheres using response surface methodology. *Chem. Eng. Res. Des.* 96, 1–14. doi:10.1016/j.cherd.2015.01.014

Dolatabadi, S., Karimi, M., Nasirizadeh, S., Hatamipour, M., Golmohammadzadeh, S., and Jaafari, M. R. (2021). Preparation, characterization and *in vivo* pharmacokinetic evaluation of curcuminoids-loaded solid lipid nanoparticles (SLNs) and nanostructured lipid carriers (NLCs). *J. Drug Deliv. Sci. Technol.* 62, 102352. doi:10.1016/j.jddst.2021.102352

Elhissi, A., Hidayat, K., Phoenix, D. A., Mwesigwa, E., Crean, S., Ahmed, W., et al. (2013). Air-jet and vibrating-mesh nebulization of niosomes generated using a particulate-based proniosome technology. *Int. J. Pharm.* 444 (1–2), 193–199. doi:10.1016/j.ijpharm.2012.12.040

El-Menshawe, S. F., Ali, A. A., Rabeh, M. A., and Khalil, N. M. (2018). Nanosized soy phytosome-based thermogel as topical anti-obesity formulation: an approach for acceptable level of evidence of an effective novel herbal weight loss product. *Int. J. Nanomedicine* 13, 307–318. doi:10.2147/ijn.s153429

Elsayed, M. M., Abdallah, O. Y., Naggar, V. F., and Khalafallah, N. M. (2006). Deformable liposomes and ethosomes: mechanism of enhanced skin delivery. *Int. J. Pharm.* 322 (1-2), 60–66. doi:10.1016/j.ijpharm.2006.05.027

Fatima, I., Rasul, A., Shah, S., Saadullah, M., Islam, N., Khames, A., et al. (2022). Novasomes as nano-vesicular carriers to enhance topical delivery of fluconazole: a new approach to treat fungal infections. *Molecules* 27 (9), 2936. doi:10.3390/molecules27092936

Gamal, A., Saeed, H., Sayed, O. M., Kharshoum, R. M., and Salem, H. F. (2020). Proniosomal microcarriers: impact of constituents on the physicochemical properties of proniosomes as a new approach to enhance inhalation efficiency of dry powder inhalers. *AAPS PharmSciTech* 21 (5), 156–12. doi:10.1208/s12249-020-01705-0

Gontijo, A. V. L., Grégoire, N., Lamarche, I., Gobin, P., Couet, W., and Marchand, S. (2014). Biopharmaceutical characterization of nebulized antimicrobial agents in rats: 2. Colistin. *Antimicrob. Agents Chemother.* 58 (7), 3950–3956. doi:10.1128/aac.02819-14

Guimarães, D., Cavaco-Paulo, A., and Nogueira, E. (2021). Design of liposomes as drug delivery system for therapeutic applications. *Int. J. Pharm.* 601, 120571. doi:10.1016/j.ijpharm.2021.120571

Günther, S., Asper, M., Röser, C., Luna, L. K., Drosten, C., Becker-Ziaja, B., et al. (2004). Application of real-time PCR for testing antiviral compounds against Lassa virus, SARS coronavirus and Ebola virus *in vitro*. *Antivir. Res.* 63 (3), 209–215. doi:10.1016/j.antiviral.2004.05.001

Gupta, P. N., Mishra, V., Rawat, A., Dubey, P., Mahor, S., Jain, S., et al. (2005). Non-invasive vaccine delivery in transfersomes, niosomes and liposomes: a comparative study. *Int. J. Pharm.* 293 (1-2), 73–82. doi:10.1016/j.ijpharm.2004.12.022

Gupta, V., and Trivedi, P. (2012). Enhancement of storage stability of cisplatin-loaded protransfersome topical drug delivery system by surface modification with block copolymer and gelling agent. *J. Drug Deliv. Sci. Technol.* 22 (4), 361–366. doi:10.1016/S1773-2247(12)50060-2

Gurwitz, D. (2020). Angiotensin receptor blockers as tentative SARS-CoV-2 therapeutics. *Drug Dev. Res.* 81 (5), 537–540. doi:10.1002/ddr.21656

Gyanewali, S., Kesharwani, P., Sheikh, A., Ahmad, F. J., Trivedi, R., and Talegaonkar, S. (2021). Formulation development and *in vitro–in vivo* assessment of protransfersomal gel of anti-resorptive drug in osteoporosis treatment. *Int. J. Pharm.* 608, 121060. doi:10.1016/j.ijpharm.2021.121060

Hameed, H., Aydin, S., and Başaran, N. (2016). Sinapic acid: is it safe for humans? *Fabad J. Pharm. Sci.* 41 (1), 39–49.

Jain, S., Jain, P., and Uma Maheshwari, R. J. N. (2003). Transfersomes—a novel vesicular carrier for enhanced transdermal delivery: develop-ment, characterization, and performance evaluation. *Drug Dev. Indus Pharm.* 29, 1013–1026. doi:10.1081/ddc-120025458

Jara, M. O., Warnken, Z. N., Sahakijpijarn, S., Moon, C., Maier, E. Y., Christensen, D. J., et al. (2021). Niclosamide inhalation powder made by thin-film freezing: multi-dose tolerability and exposure in rats and pharmacokinetics in hamsters. *Int. J. Pharm.* 603, 120701. doi:10.1016/j.ijpharm.2021.120701

Jose, S., Anju, S. S., Cinu, T. A., Aleykutty, N. A., Thomas, S., and Souto, E. B. (2014). *In vivo* pharmacokinetics and biodistribution of resveratrol-loaded solid lipid nanoparticles for brain delivery. *Int. J. Pharm.* 474 (1–2), 6–13. doi:10.1016/j.ijpharm.2014.08.003

Kern, S. M., Bennett, R. N., Mellon, F. A., Kroon, P. A., and Garcia-Conesa, M. T. (2003). Absorption of hydroxycinnamates in humans after high-bran cereal consumption. *J. Agric. Food Chem.* 51 (20), 6050–6055. doi:10.1021/jf0302299

Khan, I., Apostolou, M., Bnyan, R., Houacine, C., Elhissi, A., and Yousaf, S. S. (2020). Paclitaxel-loaded micro or nano transfersome formulation into novel tablets for pulmonary drug delivery via nebulization. *Int. J. Pharm.* 575, 118919. doi:10.1016/j.ijpharm.2019.118919

Khan, I., Needham, R., Yousaf, S., Houacine, C., Islam, Y., Bnyan, R., et al. (2021). Impact of phospholipids, surfactants and cholesterol selection on the performance of transfersomes vesicles using medical nebulizers for pulmonary drug delivery. *J. Drug Deliv. Sci. Technol.* 66, 102822. doi:10.1016/j.jddst.2021.102822

Li, J., Zhang, K., Wu, D., Ren, L., Chu, X., Qin, C., et al. (2021). Liposomal remdesivir inhalation solution for targeted lung delivery as a novel therapeutic approach for COVID-19. *Asian J. Pharm. Sci.* 16 (6), 772–783. doi:10.1016/j.ajps.2021.09.002

López, O., De La Maza, A., Coderch, L., López-Iglesias, C., Wehrli, E., and Parra, J. L. (1998). Direct formation of mixed micelles in the solubilization of phospholipid liposomes by Triton X-100. *FEBS Lett.* 426 (3), 314–318. doi:10.1016/S0014-5793(98)00363-9

Moawad, F. A., Ali, A. A., and Salem, H. F. (2017). Nanotransfersomes-loaded thermosensitive *in situ* gel as a rectal delivery system of tizanidine HCL: preparation, *in vitro* and *in vivo* performance. *Drug Deliv.* 24 (1), 252–260. doi:10.1080/10717544.2016.1245369

Nesamony, J., Shah, I. S., Kalra, A., and Jung, R. (2014). Nebulized oil-in-water nanoemulsion mists for pulmonary delivery: development, physico-chemical characterization and *in vitro* evaluation. *Drug Dev. Ind. Pharm.* 40 (9), 1253–1263. doi:10.3109/03639045.2013.814065

Opatha, S. A. T., Titapiwatanakun, V., and Chutoprapat, R. (2020). Transfersomes: a promising nanoencapsulation technique for transdermal drug delivery. *Pharmaceutics* 12 (9), 855. doi:10.3390/pharmaceutics12090855

Orfali, R., Rateb, M. E., Hassan, H. M., Alonazi, M., Gomaa, M. R., Mahrous, N., et al. (2021). Sinapic acid suppresses SARS CoV-2 replication by targeting its envelope protein. *Antibiotics* 10 (4), 420–13. doi:10.3390/antibiotics10040420

Pandi, A., and Manickam, V. (2021). Pharmacological and therapeutic applications of Sinapic acid — an updated review Oil seeds Spices Rye MyrisϴCa fragrans Salvia officinalis Berries. *Mol. Biol. Rep.* 48 (4), 3733–3745. doi:10.1007/s11033-021-06367-0

Parmar, A., Singh, K., Bahadur, A., Marangoni, G., and Bahadur, P. (2011). Interaction and solubilization of some phenolic antioxidants in Pluronic® micelles. *Colloids Surfaces B Biointerfaces* 86 (2), 319–326. doi:10.1016/j.colsurfb.2011.04.015

Pastor, M., Salomon, C. J., Esquisabel, A., and Pedraz, J. L. (2015). Pulmonary drug delivery: a review on nanocarriers for antibacterial chemotherapy. *J. Antimicrob. Chemother.* 70 (11), 2945–2955. doi:10.1093/jac/dkv192

Pierce, C. G., Uppuluri, P., Tummala, S., and Lopez-Ribot, J. L. (2010). A 96 well microtiter plate-based method for monitoring formation and antifungal susceptibility testing of Candida albicans biofilms. *J. Vis. Exp.* (44), 2287. doi:10.3791/2287

Pooladanda, V., Thatikonda, S., Muvvala, S. P., Devabattula, G., and Godugu, C. (2021). BRD4 targeting nanotherapy prevents lipopolysaccharide induced acute respiratory distress syndrome. *Int. J. Pharm.* 601, 120536. doi:10.1016/j.ijpharm.2021.120536

Saimi, N. I. M., Salim, N., Ahmad, N., Abdulmalek, E., and Rahman, M. B. A. (2021). Aerosolized niosome formulation containing gemcitabine and cisplatin for lung cancer treatment: optimization, characterization and *in vitro* evaluation. *Pharmaceutics* 13 (1), 1–19. doi:10.3390/pharmaceutics13010059

Salem, H., Abdelrahi, M., Eid, K. A., and Sharaf, M. (2011). Nanosized rods agglomerates as a new approach for formulation of a dry powder inhaler. *Int. J. nanomedicine* 6, 311–320. doi:10.2147/IJN.S14309

Salem, H. F., Ahmed, S. M., and Omar, M. M. (2016). Liposomal flucytosine capped with gold nanoparticle formulations for improved ocular delivery. *Drug Des. Devel Ther.* 10, 277–295. doi:10.2147/dddt.s91730

Salem, H. F., Kharshoum, R. M., Abou-Taleb, H. A., and Naguib, D. M. (2019a). Nanosized transferosome-based intranasal *in situ* gel for brain targeting of resveratrol: formulation, optimization, *in vitro* evaluation, and *in vivo* pharmacokinetic study. *AAPS PharmSciTech* 20 (5), 181. doi:10.1208/s12249-019-1353-8

Salem, H. F., Kharshoum, R. M., Abou-Taleb, H. A., and Naguib, D. M. (2019b). Brain targeting of resveratrol through intranasal lipid vesicles labelled with gold nanoparticles: *in vivo* evaluation and bioaccumulation investigation using computed tomography and histopathological examination. *J. Drug Target* 27 (10), 1127–1134. doi:10.1080/1061186X.2019.1608553

Salem, H. F., Kharshoum, R. M., Abou-Taleb, H. A., and Naguib, D. M. (2019c). Nanosized nasal emulgel of resveratrol: preparation, optimization, *in vitro* evaluation and *in vivo* pharmacokinetic study. *Drug Dev. Ind. Pharm.* 45 (10), 1624–1634. doi:10.1080/03639045.2019.1648500

Salem, H. F., Kharshoum, R. M., El-ela, F. I. A., F, A. G., and Abdellatif, K. R. A. (2018). Evaluation and optimization of pH - responsive niosomes as a carrier for efficient treatment of breast cancer. *Drug Deliv. Transl. Res.* 8 (3), 633–644. doi:10.1007/s13346-018-0499-3

Shakeel, F., Haq, N., Raish, M., Anwer, M. K., and Al-Shdefat, R. (2016a). Solubility and thermodynamic analysis of sinapic acid in various neat solvents at different temperatures. *J. Mol. Liq.* 222, 167–171. doi:10.1016/j.molliq.2016.07.007

Shakeel, F., Raish, M., Anwer, M. K., and Al-Shdefat, R. (2016b). Self-nanoemulsifying drug delivery system of sinapic acid: *in vitro* and *in vivo* evaluation. *J. Mol. Liq.* 224, 351–358. doi:10.1016/j.molliq.2016.10.017

Song, C. K., Balakrishnan, P., Shim, C. K., Chung, S. J., Chong, S., and Kim, D. D. (2012). A novel vesicular carrier, transethosome, for enhanced skin delivery of voriconazole: characterization and *in vitro/in vivo* evaluation. *Colloids surfaces. B, Biointerfaces* 92, 299–304. doi:10.1016/j.colsurfb.2011.12.004

Song, F. fan, jun, T. S., long, Y. G., and Sun, X. yang (2022). Effect of phospholipid/flaxseed oil ratio on characteristics, structure change, and storage stability of liposomes. *LWT* 157, 113040. doi:10.1016/j.lwt.2021.113040

WHO (2024). WHO updates list of drug-resistant bacteria most threatening to human health. Available online at: https://www.who.int/news/item/17-05-2024-who-updates-list-of-drug-resistant-bacteria-most-threatening-to-human-health.

Yusuf, A. H., Ali, A. A., Orr, N., Helen, O., Kett, V. L., Yusuf, H., et al. (2017). Novel freeze-dried DDA and TPGS liposomes are suitable for nasal delivery of vaccine. *Int. J. Pharm.* 533 (1), 179–186. doi:10.1016/j.ijpharm.2017.09.011

Zhong, B., Robinson, N. A., Warner, R. D., Barrow, C. J., Dunshea, F. R., and Suleria, H. A. R. (2020). LC-ESI-QTOF-MS/MS characterization of seaweed phenolics and their antioxidant potential. *Mar. Drugs* 18 (6), 331. doi:10.3390/md18060331